FOURIER DISSECTION OF EARLY-TYPE GALAXY BARS

R. BUTA,[1] E. LAURIKAINEN,[2] H. SALO,[2] D. L. BLOCK,[3] AND J. H. KNAPEN[4]

ABSTRACT

This paper reports on a near-infrared survey of early-type galaxies designed to provide information on bar strengths, bulges, disks, and bar parameters in a statistically well-defined sample of S0–Sa galaxies. Early-type galaxies have the advantage that their bars are relatively free of the effects of dust, star formation, and spiral structure that complicate bar studies in later type galaxies. We describe the survey and present results on a detailed analysis of the relative Fourier intensity amplitudes of bars in 26 early-type galaxies. We also evaluate the "symmetry assumption" of these amplitudes with radius, used recently for bar-spiral separation in later type galaxies. The results show a wide variety of radial Fourier profiles of bars, ranging from simple symmetric profiles that can be represented in terms of a single Gaussian component to both symmetric and asymmetric profiles that can be represented by two overlapping Gaussian components. More complicated profiles than these are also found, often due to multiple barlike features including extended ovals or lenses. Based on the gravitational bar torque indicator Q_b, double-Gaussian bars are stronger on average than single-Gaussian bars, at least for our small sample. We show that published numerical simulations in which the bar transfers a large amount of angular momentum to the halo can account for many of the observed profiles. The range of possibilities encountered in models seems well-represented in the observed systems.

Key words: galaxies: kinematics and dynamics — galaxies: photometry — galaxies: spiral — galaxies: structure

1. INTRODUCTION

S0 galaxies were introduced to the Hubble sequence by Hubble (1936) as a means of bridging the apparently catastrophic gap between E7 and Sa galaxies. After real examples were discovered (see Sandage 1961), the hallmark of the class became a disk shape (definitely "later than" E6 or E7) and an absence of spiral arms or star formation. SB0 galaxies were originally classified as SBa by Hubble (1926), even though they also lacked arms. This inconsistency was corrected in Sandage (1961).

Barred S0 galaxies are extremely interesting because they help to take some of the mystery out of S0 galaxies in general: a bar is usually a disk feature that is closely related to spiral structure in many galaxies (e.g., Kormendy & Norman 1979). In addition, ring features are directly related to bars in spiral galaxies, and SB0 galaxies may show vestiges of similar rings. One could therefore ask whether bar properties in S0 galaxies might provide any clues as to how S0 and spiral galaxies might be related in an evolutionary sense.

We are interested in the distribution of bar strengths in S0 galaxies, a property of very early–type galaxies that has not yet been tapped for what it might tell us about the evolutionary history of S0 galaxies. Early-type galaxies have a remarkable array of bar morphologies whose Fourier and other properties are worth characterizing in more detail. The advantage we have for examining these issues is that early-type galaxies show their bars largely unaffected by dust, star formation, and spiral structure. We can look for subtle structural differences between different bars and isolate possible different bar types.

We are also interested in comparing early-type barred galaxies with the models of Athanassoula (2003, 2005), who demonstrated the importance of angular momentum transfer to the halo as a means of producing strong bars. The Fourier profile information we provide here is ideally suited to comparison with n-body models and for evaluating the symmetry assumption used for bar-spiral separation (Buta et al. 2003).

The Near-Infrared S0 Survey (NIRS0S) is an attempt to obtain a statistically well-defined database of images of S0 galaxies from which the properties of S0 bars may be fairly compared to those of spiral galaxies. The Ohio State University Bright Galaxy Survey (OSUBGS; Eskridge et al. 2002) provides a valuable data set for studying the properties of spiral galaxies and has been fully tapped for bar-strength studies by Block et al. (2002), Buta et al. (2004, hereafter BLS04), Laurikainen et al. (2004a, 2004b), and Buta et al. (2005). The questions we address with the NIRS0S sample are the following: (1) How strong do S0 bars get compared to spiral bars? (2) How does the distribution of bar strengths in S0 galaxies compare with that for spiral galaxies? (3) What characterizes the morphology of bars in S0 galaxies? And (4) what are the near-IR luminosity ratios and profile characteristics of bulges in S0 galaxies?

In describing early-type disk galaxies, we use specific terminology. An "ansae" bar is one showing bright enhancements near the ends (Sandage 1961). A "regular" bar does not show such enhancements. Ansae bars are preferentially found in early-type galaxies, while regular bars are preferentially found in later types, although no statistical study has quantified the difference. A "lens" is a feature showing a shallow brightness gradient interior to a sharp edge (Kormendy 1979). An "oval" is a broad elongation in the light distribution; it differs from a conventional bar in lacking higher order Fourier terms. If intrinsically elongated, a lens can also be an oval. Ovals are discussed further by Kormendy & Kennicutt (2004).

In this paper we focus on a set of 26 galaxies from the NIRS0S having ovals and/or bars and investigate radial profiles of relative Fourier intensity amplitudes. We seek to examine the diversity in early-type bars according to the symmetry of such profiles.

[1] Department of Physics and Astronomy, University of Alabama, Box 870324, Tuscaloosa, AL 35487.
[2] Division of Astronomy, Department of Physical Sciences, University of Oulu, Oulu FIN-90014, Finland.
[3] School of Computational and Applied Mathematics, University of the Witwatersrand, Johannesburg, South Africa.
[4] Centre for Astrophysics Research, University of Hertfordshire, Hatfield AL10 9AB, UK.
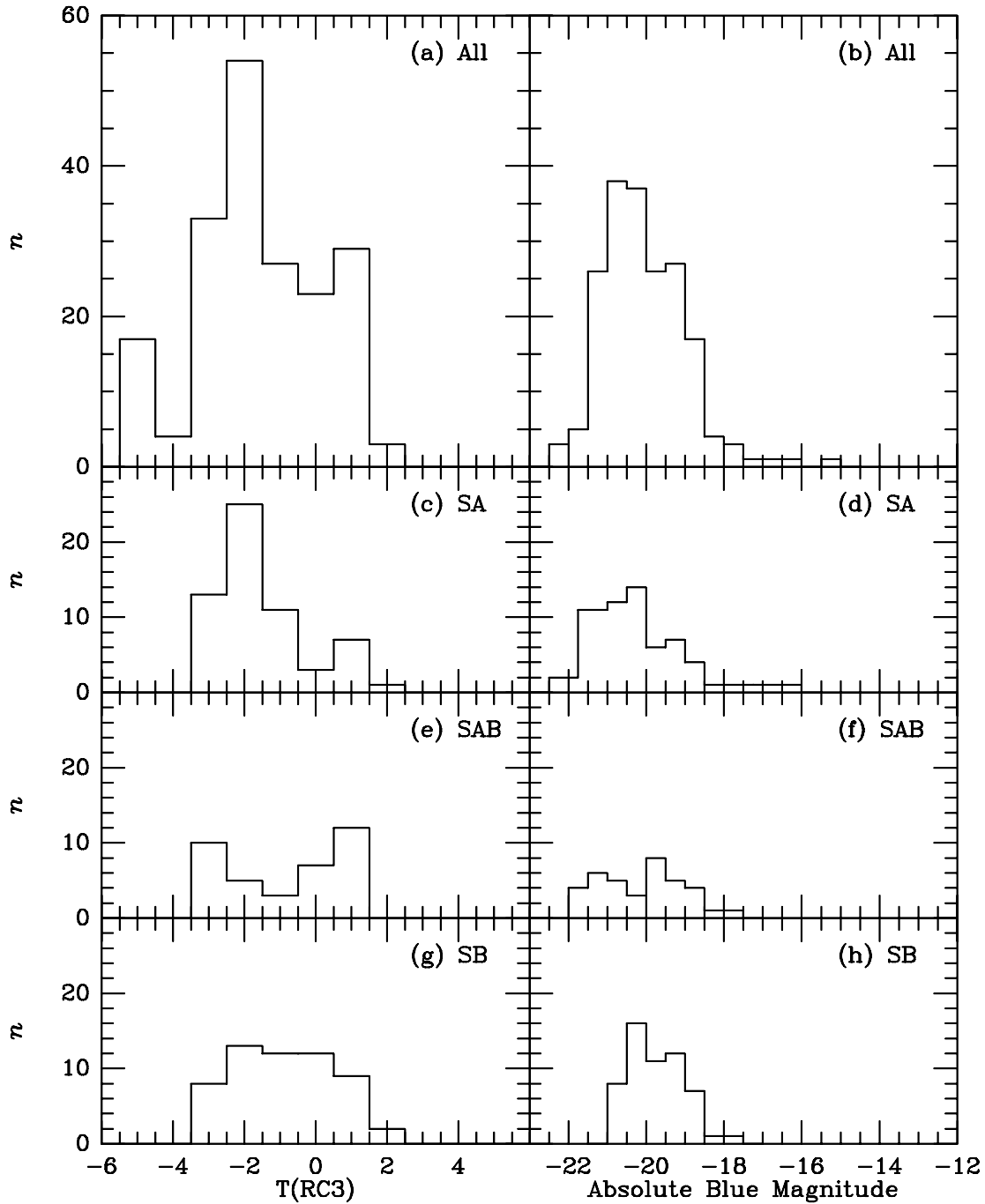
Fig. 1.—Histograms of numbers of NIRS0S galaxies vs. RC3-type index T and absolute blue magnitude M_B^o based on RC3 data and distances (mainly from Tully 1988) using a Hubble constant of 75 km s^{-1} Mpc^{-1}. The top two panels are for the full sample, while the lower ones are divided according to RC3 family.

In § 2 we describe the rationale for the survey and the sample selection criteria. In § 3 we describe the observations made with different instruments and detectors. The study of the relative Fourier intensity amplitudes is presented in § 5. A discussion of the results is presented in § 6.

2. SAMPLE CHARACTERISTICS AND NATURE OF THE SURVEY

The sample for the NIRS0S has been drawn from the Third Reference Catalog of Bright Galaxies (RC3; de Vaucouleurs et al. 1991). We selected all galaxies in the revised type range $-3 \leq T < 2$ (S0$^-$ to Sa) having $B_T \leq 12.5$ and $\log R_{25} \leq 0.35$ as

targets for the survey, which amounts to 170 galaxies. However, any sample of S0 galaxies is bound to have a bias in the sense that some nonbarred S0 galaxies lacking any distinct structure will likely be classified as elliptical galaxies. This could have serious effects on a bar-strength study. To reduce the bias somewhat, we have supplemented the sample with 20 more galaxies that are classified as E or E$^+$ in RC3 but that are shown by Sandage & Bedke (1994, hereafter SB94) to be S0 galaxies. In these cases, we believe the SB94 types to be more accurate. Related to this issue is the possibility that some galaxies classified as S0 in RC3 are actually E galaxies. This is shown to be the case with two of our ESO sample galaxies (Laurikainen et al. 2006,

Sample	$\langle M_B^o \rangle$	$\langle T \rangle$ (RC3)	N
Full sample............	-20.044 ± 0.078	-1.595 ± 0.128	190
SA galaxies	-20.114 ± 0.151	-1.530 ± 0.165	60
SAB galaxies	-20.129 ± 0.175	-0.846 ± 0.272	37
SB galaxies	-19.735 ± 0.094	-0.905 ± 0.184	56

Note.—Based on RC3 data and distances either from Tully (1988) or estimated using the linear Virgocentric flow model of Aaronson et al. (1982) and a Hubble constant of 75 km s^{-1} Mpc^{-1}.

hereafter Paper III). In order to identify such cases, we have to rely on the multicomponent decompositions.

Another potential problem in an early-type disk galaxy sample is the misclassification of edge-on disks as bars, something that could happen if an edge-on disk is immersed in a significant bulge component or if the disk is a polar ring. Detailed analysis should identify such cases.

The sample selection criteria do not perfectly match those of the OSUBGS because S0 galaxies are not as abundant in RC3 as are spiral galaxies for the OSUBGS selection criteria (mainly $B_T \leq 12.0$). We decided it was more important to try and match the *sample size* of the OSUBGS rather than the exact selection criteria. Although the OSUBGS had no restriction on log R_{25}, we imposed such a restriction on our S0 sample because bar strengths cannot be derived reliably for highly inclined galaxies.

The rationale for observing S0 galaxies in the near-IR requires some discussion. Although both S0 and spiral galaxies are highly flattened disk-shaped systems, S0 galaxies mostly lack spiral structure and star formation. By default, such systems tend also to be low in dust content. This means that, in principle, bar strengths in S0 galaxies could be derived in optical bands with little impact due to dust. The reason we chose not to follow such an approach is that we wanted to make a fair comparison between bars in S0 and in spiral galaxies. In optical bands, bars in spiral galaxies may be affected by star formation, leading dust lanes, and even more disorganized dust lanes, such that the kind of analysis we describe here is less effective for determining bar properties. These effects are minimized or eliminated in the near-IR, and thus to make the comparison with spiral galaxies fair it is essential that the S0 galaxies also be observed in the near-IR. In addition, some S0 galaxies do have dust, and the impact of this dust is minimized in the near-IR passbands.

Figure 1 shows how our sample galaxies are distributed in type, family, and absolute B-band magnitude. Figure 1a shows that the dominant type is $T = -2$, or S0^o. A significant fraction of these have no family estimate in RC3, but among those that do, those classified as type SA0^o contribute the most to the $T = -2$ peak. The unusual distribution for the SAB galaxies in the sample is partly due to classification uncertainties, as noted by de Vaucouleurs (1963). SB galaxies in the sample are more uniformly distributed across the type bins.

Table 1 summarizes mean absolute B-band magnitudes and RC3 types for the same samples as illustrated in Figure 1. The average absolute magnitude for the full sample is comparable to that for the spiral sample used by BLS04. Most noteworthy is that the SB galaxies in the NIRS0S sample have a fainter average absolute magnitude than the SA and SAB galaxies, the difference being significant at the 2 σ level. Also, the SAB and SB galaxies are on average of later type than the SA galaxies (3 σ level). The sample is still biased in much the same way as the OSUBGS

sample of spiral galaxies (BLS04), with few galaxies having $M_B > -18$.

3. OBSERVATIONS

Observations related to NIRS0S have been taken at the Nordic 2.5 m Optical Telescope (NOT) in 2003 January and September and 2004 January and with the ESO 3.5 m New Technology Telescope (NTT) in 2004 December. The NOT observations were made with NOTCam, a multimode instrument that can provide images in the 1–2.5 μm region. We used it to observe 45 galaxies in wide-field imaging mode, which provided a $4' \times 4'$ field of view with 0″.23 pixels. Flat-fielding was accomplished with twilight frames. All of the NOT galaxies were observed in the 2.15 μm K-short (K_s) band, whose wavelength cutoff, shorter than the regular K-band, reduces some of the thermal background component. (See Persson et al. [1998] for a discussion of this filter and its relation to the regular Johnson K filter.) In some cases, we also observed an object in the J-band (1.25 μm) in order to use color gradients to evaluate the constancy of the stellar mass-to-light ratio used in gravitational torque analyses (Quillen et al. 1994). Other aspects of the data reduction are described by Laurikainen et al. (2005, hereafter Paper I).

The NTT observations were made with SofI, a wide-field IR spectroimager designed for the 1–2.5 μm region. We used SofI to image 15 galaxies with a field of view of $4'.9 \times 4'.9$ and a pixel size of 0″.29. As with NOTCam, the SofI observations were made with a K_s filter supplemented in a few cases with a J-band filter. The reductions for this data set are described by Paper III.

The galaxies observed up to the time of the present analysis were selected by observing conditions and the time of year and should be a representative subset of the whole NIRS0S. A few galaxies outside the NIRS0S sample are included in the present data set because some of our NOT runs were carried out under precarious conditions of wind and seeing that limited our access to NIRS0S sample galaxies. In this circumstance, we relaxed our magnitude limit somewhat to accommodate other accessible objects.

4. MULTICOMPONENT DECOMPOSITIONS AND DEPROJECTED IMAGES

Paper I has analyzed 24 of the NOT galaxies observed for our survey. A decomposition analysis of the ESO sample is provided in Paper III. In addition to providing new information on the bulge and disk properties of S0 galaxies, these studies also have provided deprojected images, constructed using orientation parameters based, when possible, on deep optical images. The deprojected images are corrected for bulge deprojection stretch by using the decompositions to remove the bulge, deprojecting the disk alone, and then adding back the bulge as a spherical component. The decompositions were essential because relative Fourier intensity profiles would be affected if bulge shapes were ignored. With corrected images we can reliably analyze these profiles for as much intrinsic information as possible. Paper I and Paper III list the orientation parameters used for our deprojections.

Note that in some cases the deprojection procedure fails because the bulge has a flattening intermediate between a sphere and a highly flattened disk. This is manifested as undercorrected light along the galaxy minor axis, leaving zones deficient in light that distort the inner parts of the bar. For our analysis here we do not use those galaxies (NGC 1350, 3626, and 4340) in our present sample where these deficient zones appeared to be significant. For one of these cases (NGC 1079), we used deprojected images in which the bulge is assumed to be as flat as the disk. This left

Galaxy (1)	Type (2)	$\log D_o$ (3)	M_B^o (4)	μ_o (5)	Telescope (6)
NGC 718.......	(R′)SA<u>B</u>(rs)a	1.38	−19.4	31.65	NOT
NGC 936.......	SB(rs)0⁺	1.67	−20.8	31.14	NOT
NGC 1022.....	(R)SB(<u>r</u>s)a pec	1.38	−19.4	31.33	NOT
NGC 1079.....	(R₁R′₂)SA<u>B</u>(rs)a	1.53	−19.0	31.13	NTT
NGC 1302.....	(R′₂)SA<u>B</u>(rs)0/a	1.59	−20.0	31.51	NOT
NGC 1317.....	SAB(r)a	1.44	−19.3	31.14	NTT
NGC 1326.....	(R₁)SAB(r)0/a	1.57	−19.9	31.14	NTT
NGC 1387.....	SB0⁻	1.45	−18.4	31.14	NTT
NGC 1440.....	SB(s)0⁺	1.34	−18.9	31.30	NOT
NGC 1452.....	(R′)SB(r)a	1.36	−19.2	31.59	NOT
NGC 1512.....	SB(r)ab	1.95	−18.9	29.90	NTT
NGC 1533.....	(RL)SB0ᵒ	1.43	−19.9	30.64	NTT
NGC 1574.....	SB0⁻	1.52	−20.0	30.64	NTT
NGC 2217.....	(R)SB(rs)0/a	1.66	−20.1	31.45	NOT
NGC 2273.....	(RR)SAB(rs)a	1.54	−20.3	32.26	NOT
NGC 2681.....	(R)S<u>A</u>B(rs)0/a	1.57	−20.3	30.62	NOT
NGC 2781.....	(R′₂)SAB(rs)0/a	1.45	−19.9	32.20	NOT
NGC 2787.....	SB(r)0⁺	1.48	−19.2	30.58	NOT
NGC 2859.....	(R)SB(rl)0⁺	1.62	−20.4	32.03	NOT
NGC 2983.....	(L)SB(s)0⁺	1.38	−19.6	32.19	NOT
NGC 3081.....	(R₁R′₂)SAB(r)0/a	1.33	−20.0	32.56	NTT
NGC 3941.....	SB(s)0ᵒ	1.52	−20.2	31.38	NOT
NGC 4245.....	SB(r)0/a	1.46	−17.9	29.93	NOT
NGC 4596.....	SB(rs)0/a	1.58	−19.6	31.13	NOT
NGC 4608.....	SB(r)0/a	1.49	−19.2	31.13	NOT
NGC 4643.....	SB(rl)0/a	1.49	−20.6	32.05	NOT

NOTES.—Col. (1): Galaxy name. Col. (2): New B-band morphological classification from the de Vaucouleurs Atlas of Galaxies (Buta et al. 2006), except for NGC 1440, 2781, 2787, and 3941, whose types are in the same system but based on inspection of photographic images in Sandage & Bedke (1994). Col. (3): Logarithm of isophotal diameter at $\mu_B = 25.00$ mag arcsec^{-2}, corrected for extinction and inclination (from RC3). Col. (4): Absolute B-band magnitude based on RC3 data. Col. (5): Distance modulus from Tully (1988), which is based on a Hubble constant of 75 km s^{-1} Mpc^{-1} in conjunction with a linear Virgocentric flow model (Aaronson et al. 1982). Col. (6): Telescope used for near-IR imaging: NOT = Nordic Optical 2.5 m Telescope; NTT = ESO 3.5 m New Technology Telescope.

some "deprojection stretch" amplitude in the inner regions but had little effect on the bar. Also, those galaxies having little or no bar are not included. This left 26 galaxies for our Fourier study.

Table 2 summarizes types, diameters, distance moduli (Tully 1988), and absolute B-band magnitudes of these 26 galaxies. Unlike the types used in Table 1 and Figure 1, these are new classifications taken mostly from the de Vaucouleurs Atlas of Galaxies (Buta et al. 2006) and are based on deep optical CCD images, with the exceptions of NGC 1440, 2781, 2787, and 3941, whose types R. Buta has estimated from photographs in Sandage & Bedke (1994). The classifications are in a modified version of the de Vaucouleurs (1959) revised Hubble-Sandage system (Buta 1995). We use these classifications here because some are more accurate than RC3 classifications. Several galaxies in Table 2 that are classified as types S0ᵒ or S0⁺ in RC3 are actually early-type spiral galaxies. The average revised T index of the 26 galaxies on the RC3 numerical scale is −0.3, or type S0/a. Thus, this particular subset of the NIRS0S sample is dominated by early-type transitional spiral galaxies.

5. RELATIVE FOURIER INTENSITY PROFILES OF SB0-SBa BARS

The NIRS0S database as of this writing does not have enough galaxies to reliably tell us about the distribution of bar strengths in early-type disk galaxies, but the sample is large enough to allow us to investigate a simple characteristic of SB0 bars: the behavior of their relative Fourier intensity amplitudes and phases with radius. This is an important issue because (1) only for early-type galaxies can the Fourier properties of bars be studied largely unaffected by spiral structure; (2) the resulting Fourier profiles have the potential for allowing us to categorize bars with different Fourier characteristics; and (3) the same kind of analysis can be applied to n-body model bars (e.g., Athanassoula 2003).

A particular question we ask in this paper is this: do SB0 galaxies support the symmetry assumption used in bar-spiral separation? That is, do the relative Fourier intensity amplitudes of all even m-terms decline radially past a maximum in the same or a similar manner as they rise to that maximum? Buta et al. (2003, hereafter BBK03) showed that bars can be effectively separated from spirals using this kind of assumption. With the symmetry assumption, bars can be extrapolated into spiral-dominated regions and removed from an image. If one adds the axisymmetric background to the mapped bar image, then the strength of the bar alone can be estimated without the influence of spiral torques. Using this approach, Buta et al. (2005) were able to derive the distribution of true bar strengths (rather than total nonaxisymmetry strengths) for nearly 150 galaxies in the OSUBGS. Although the symmetry assumption had some support in previous optical studies of barred galaxies (e.g., Ohta et al. 1990), it can only be reliably evaluated if a bar is clean, i.e., not affected by dust or spiral structure. The NIRS0S is therefore ideal for validating this approach.

Our subset of 26 NIRS0S galaxies includes only those observed so far having conspicuous bars or ovals. The deprojected K_s-band images of these galaxies are shown in Figure 2. These are displayed mainly to reveal the primary bars and ovals but not necessarily secondary bars or ovals, the discussion of which is covered in more detail in Paper I and Paper III. We find a variety of Fourier properties of bars. Our main result is that the relative Fourier intensity profiles of bars in SB0 galaxies can be represented in simple ways, ranging from symmetric single-component bars, through symmetric multicomponent bars, to asymmetric multicomponent bars. We discuss the implications of these findings for the bar-halo interaction scenario proposed by Athanassoula (2003, 2005).

5.1. Fourier Profiles

Figure 3 shows plots of the relative Fourier intensities I_m/I_0 and phases ϕ_m for our subset of 26 NIRS0S galaxies. Although we computed these profiles for all even Fourier terms to $m = 20$, Figure 3 shows only the I_m/I_0 profiles for $m = 2, 4, 6,$ and 8 and ϕ_m profiles for $m = 2$ and 4. The latter sometimes show sharp changes in phase due merely to the $360°/m$ periodicity of the terms.

We can make a few general observations concerning these profiles. First, considering that these are near-IR images of early-type disk galaxies, the profiles of many are surprisingly complex. Second, more than two-thirds of the galaxies show small peaks in $m = 2$ amplitude near the center that are in some cases weak nuclear ovals or secondary bars. These features are almost never aligned with the primary bar according to the phase plots. Third, the $m = 2$ profiles are often more complicated than the $m > 2$ profiles, showing extra components in the nonaxisymmetric light distribution.

Interpreting the nuclear features requires some caution. The Fourier profiles are derived from deprojected images in which the bulge stretch has been corrected but only to the extent of approximating the bulge as a spherically symmetric light distribution. In the final fits of the decompositions described in Paper I
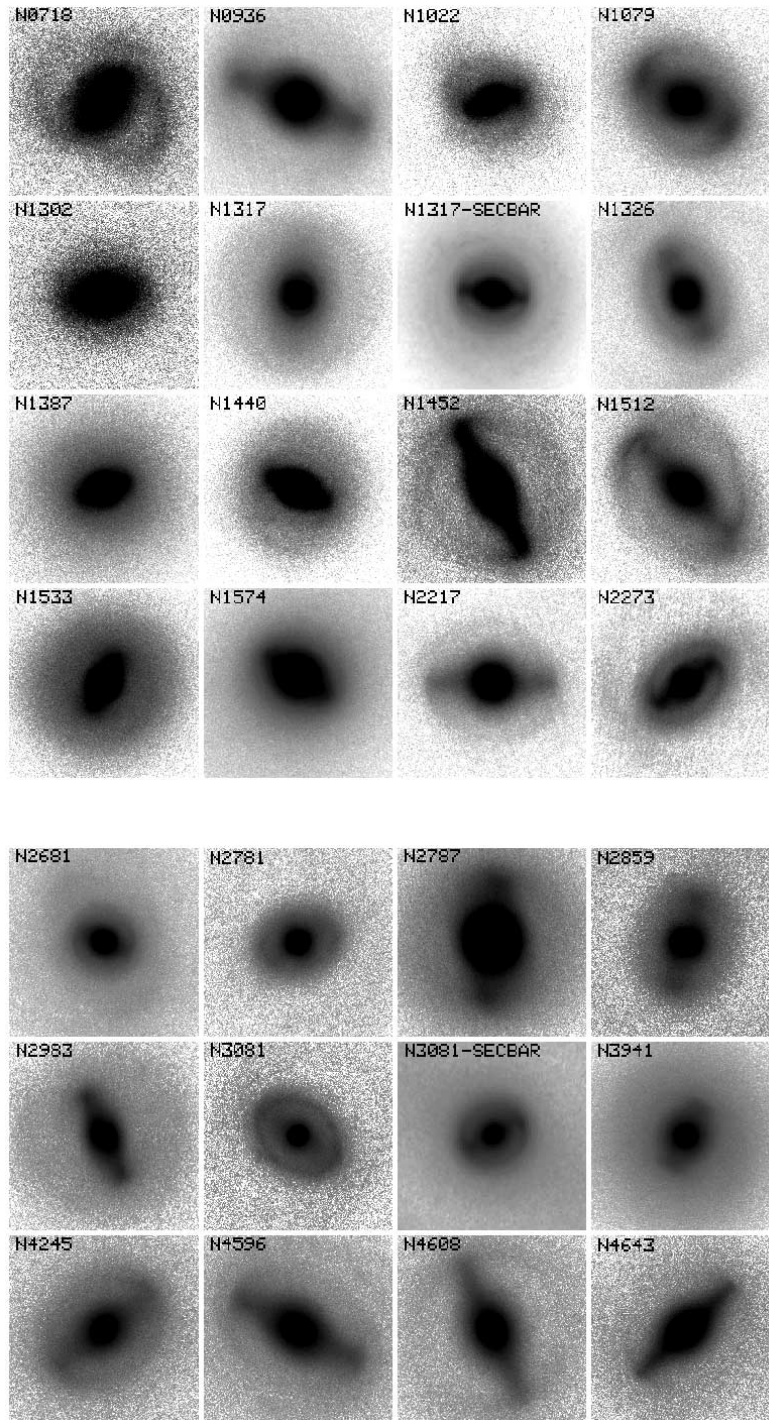
Fig. 2.—Deprojected K_s-band images of 26 NIRS0S galaxies. These are displayed mostly to emphasize the primary bars and outer disks but not necessarily any nuclear structure. The exceptions are the secondary bars of NGC 1317 and 3081, indicated by "SECBAR." The dimensions of each square are $1\rlap{.}'96 \times 1\rlap{.}'96$, except for the following: NGC 1079, 1317, 1326, 1533, and 3081 ($2\rlap{.}'47 \times 2\rlap{.}'47$); NGC 2781, 2859, 4596, and 4643 ($2\rlap{.}'73 \times 2\rlap{.}'73$); NGC 1512 ($3\rlap{.}'44 \times 3\rlap{.}'44$); and the secondary bar close-ups of NGC 1317 and 3081 ($0\rlap{.}'62 \times 0\rlap{.}'62$).

and Paper III, most of the bulges were described by elongated light distributions. Thus, the reliability of the $m = 2$ profiles and phases for the identification of central components is questionable in some cases. Although we analyze the secondary bars in NGC 1317 and 3081 in the present paper, we refer to Paper I and Paper III for detailed discussions of the other nuclear features.

Most notable in the Fourier plots are the galaxies whose bar profiles are exceptionally symmetric. Cases such as NGC 936,

1326, 1387, 1440, 1533, 1574, 2217, 2787, 2983, 3941, 4596, and 4608 have primary bars that are symmetric enough that if these bars coexisted with a spiral, the symmetry assumption would recover the bar reliably (§ 5.7).

The remaining galaxies show more complicated profiles with evidence for multiple components. In some cases, these components almost do not overlap, as in NGC 1317, 1574, 2681, 2781, and 3081. In each of these cases there is an inner component
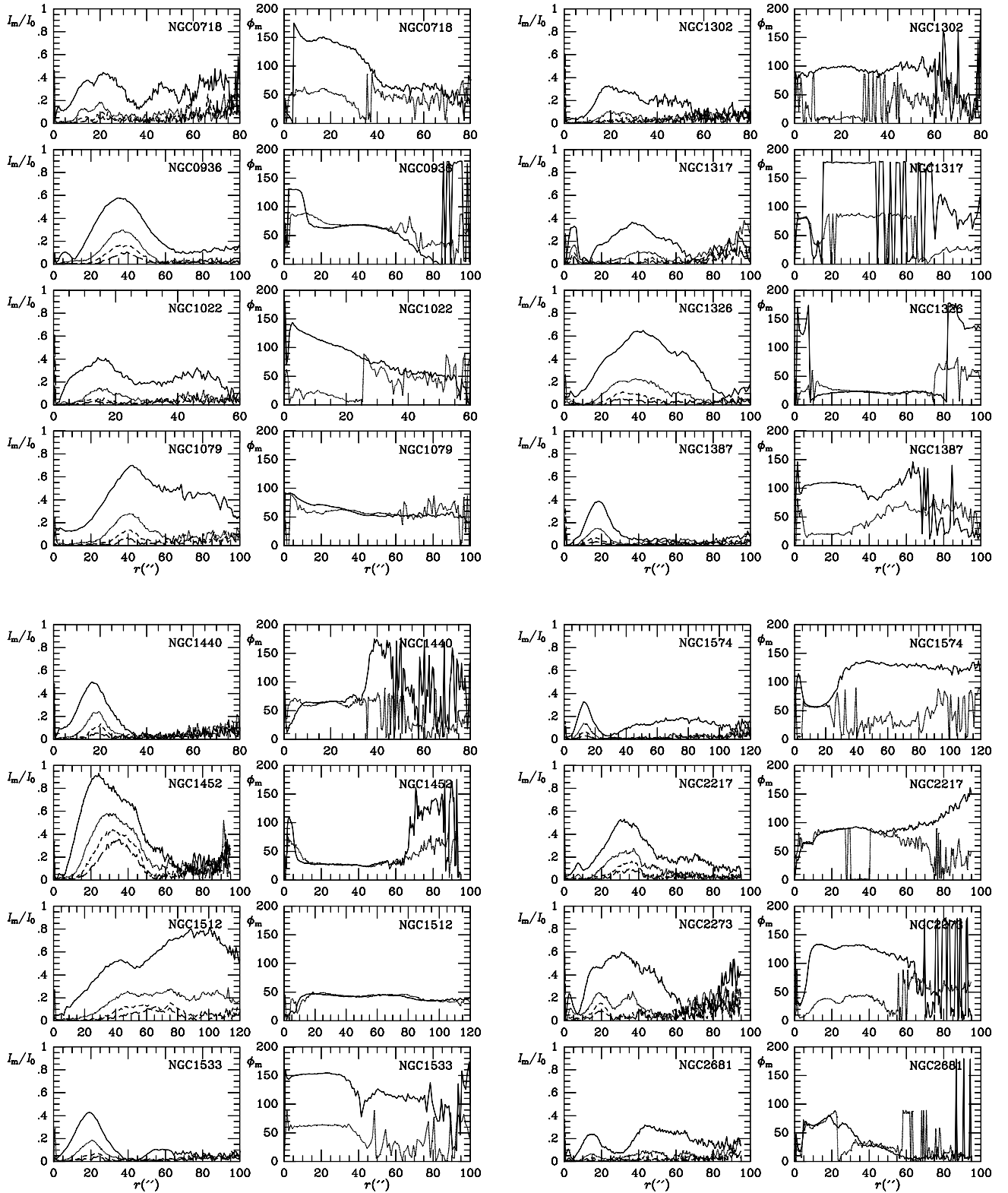
Fig. 3.—Relative Fourier intensity and phase profiles for 26 early-type disk galaxies. The left panels show the I_m/I_0 profiles for $m = 2$ (*solid curves*), $m = 4$ (*dotted curves*), $m = 6$ (*short-dashed curves*), and $m = 8$ (*long-dashed curves*). The right panels show the phases ϕ_m for $m = 2$ (*solid curves*) and $m = 4$ (*dotted curves*). The $360°/m$ periodicity causes the sharp changes in phase in many of the plots.
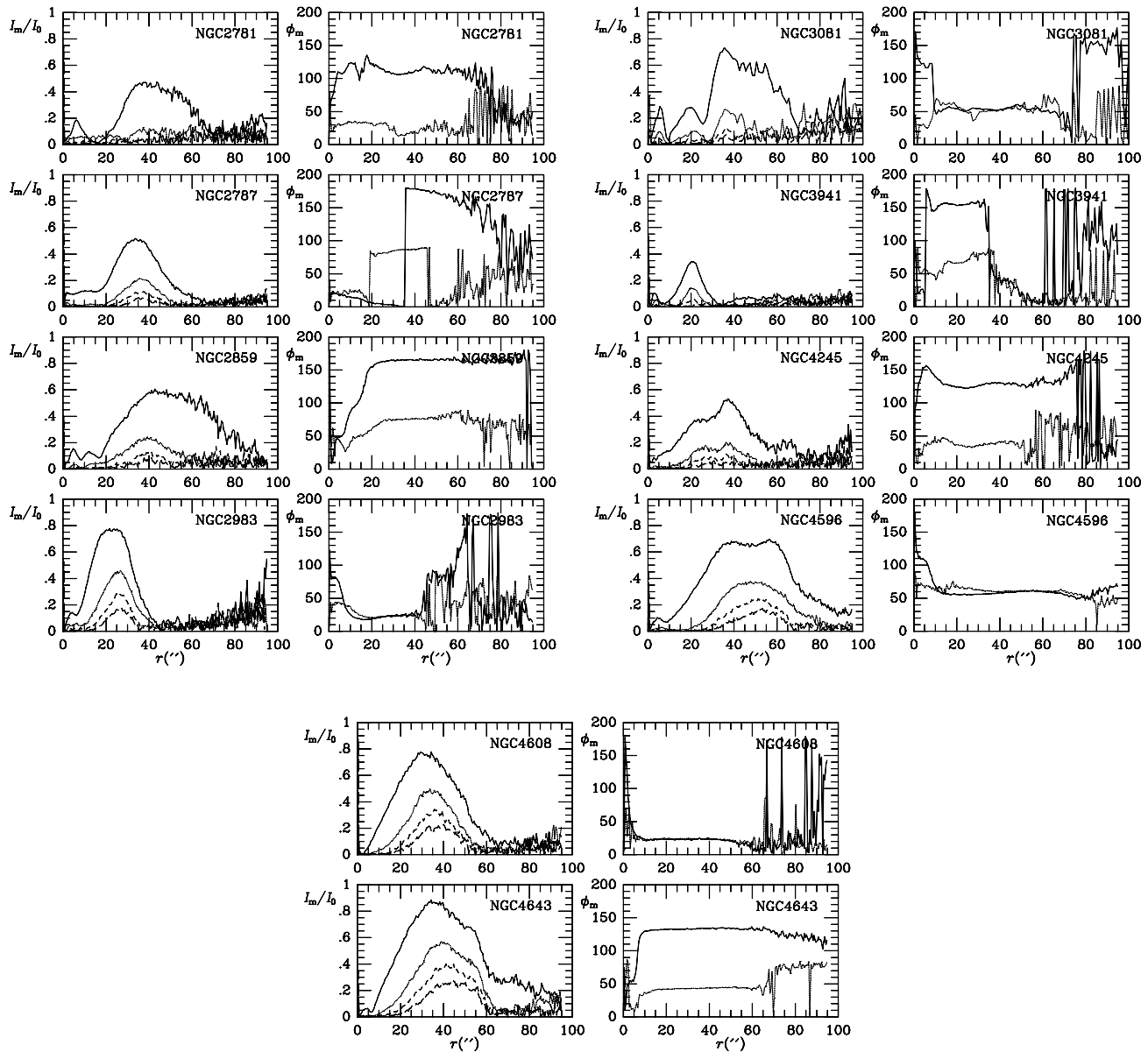
FIG. 3.—*Continued*

whose I_m/I_0 profiles are symmetric but whose outer profiles may or may not be symmetric. Other galaxies simply have asymmetric profiles for a variety of reasons. In § 5.2 we attempt to interpret the structure of each bar in the sample.

5.2. *Gaussian Components*

The appearance of many of the profiles in Figure 3 suggests that single or multiple Gaussians in fixed position angles could represent the relative Fourier intensity profiles of bars. This provides a convenient way of specifying the radial behavior of bars that could be useful for comparisons with *n*-body simulations. Figure 4 shows our Gaussian fits to all the main profiles in the sample. These were obtained via nonlinear least squares using several routines from Press et al. (1986). In addition, Figure 5 shows reconstructed images of the mapped bars (excluding the $m = 0$ term), while Figure 6 shows the light remaining after the bar model and the $m = 0$ term are subtracted. The appearance of these plots depends on how many terms were needed to repre-

sent the bar. Weak bars or ovals required only a few terms, while strong bars were mapped with all even terms to $m = 20$. The residual images include all odd Fourier terms, as well as any even terms not part of the mapped bar. The bar mappings use average phases for each term over a range of radii.

5.2.1. *Single-Gaussian Fourier Profiles*

Figure 4 shows that some observed bars have I_m/I_0 profiles that are well-fitted by a single Gaussian in all terms, with little or no amplitude outside this component. The bars seen in NGC 1387, 1440, 1533, 2787, and 3941 are like this. Related are cases such as NGC 1574 and 2681, in which an extended oval is both misaligned with and mostly outside the main bar. In these cases, the single-Gaussian characteristic still applies to the primary bar, which is mostly separate from the oval. NGC 2217 may also be in this category, although it has a significant secondary bar and a faint outer ring, and its profiles are less regular in appearance.
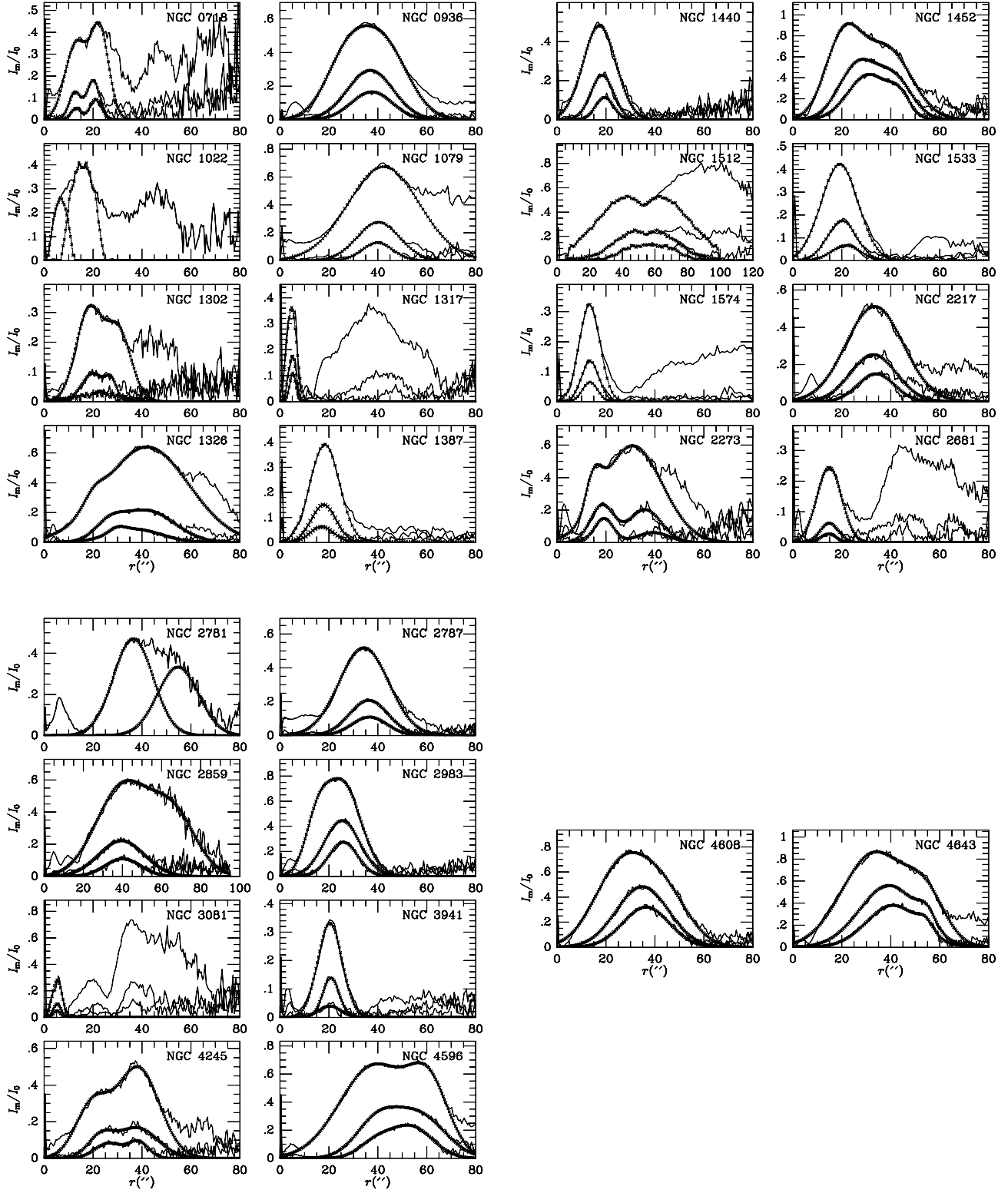
FIG. 4.—Gaussian representations of the $m = 2$, 4, and 6 I_m/I_0 profiles of the same galaxies as in Fig. 3. Crosses show the fits. In NGC 1022 and 1512, the crosses are based on the symmetry assumption, not Gaussian fits. For NGC 2781, the two Gaussians are in slightly different position angles and are shown separately. Higher order terms than $m = 6$ could also be fitted similarly but are not shown. Only the $m = 2$ term is shown for NGC 1022 and 2781.
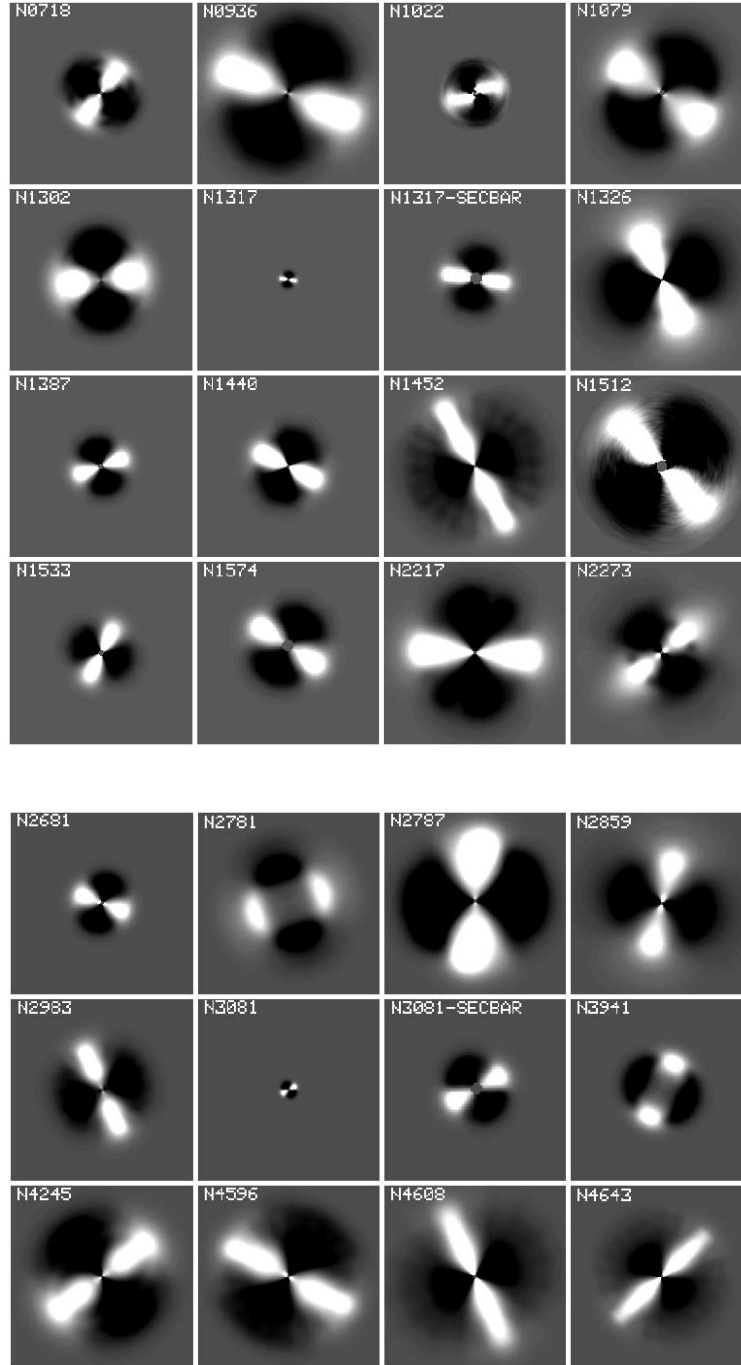
FIG. 5.—Reconstructed images of the bars of the 26 galaxies based on the Gaussian or symmetry assumption representations shown in Fig. 4. Only even Fourier terms up to a maximum m_{max} were used depending on the strength of the bar. For the strongest bars in the sample, $m_{max} = 20$. The dimensions of each square are the same as in Fig. 2.

FIG. 6.—Residual $m > 0$ images of the 26 galaxies on the same scales as in Fig. 5. These include even and odd Fourier terms up to $m_{\max} = 20$ as needed. These maps show asymmetries, extra barlike features in the center, and the imperfections of some of the Gaussian fits. The dimensions of each square are the same as in Fig. 2.

TABLE 3
GAUSSIAN FOURIER COMPONENTS FOR 24 EARLY-TYPE BARRED AND OVAL GALAXIES

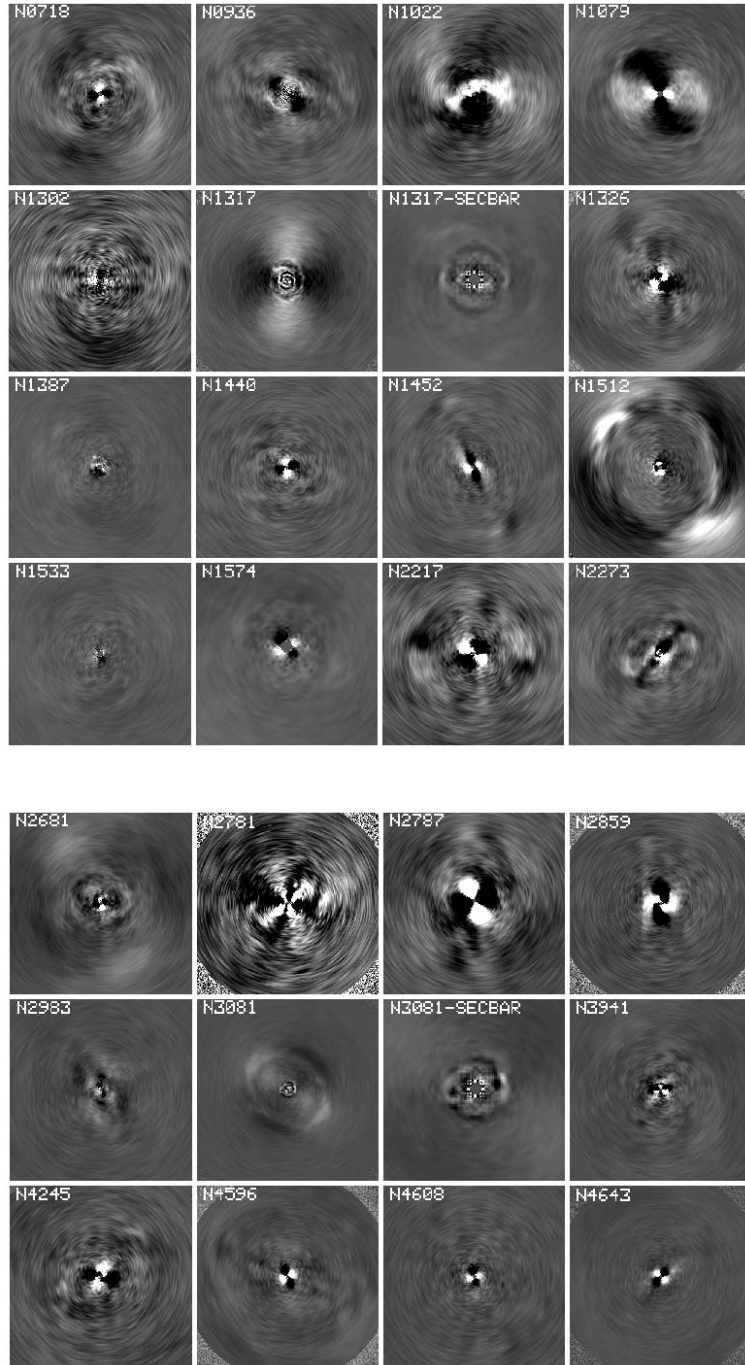| Galaxy (1)	A_2 (2)	A_4 (3)	A_6 (4)	A_8 (5)	r_2 (arcsec) (6)	r_4 (arcsec) (7)	r_6 (arcsec) (8)	r_8 (arcsec) (9)	σ_2 (arcsec) (10)	σ_4 (arcsec) (11)	σ_6 (arcsec) (12)	σ_8 (arcsec) (13)	r_2/r_o (14)
N0718-1	0.35	0.12	0.05	0.00	13.1	12.6	13.1	0.0	4.5	2.4	2.1	0.0	0.18
N0718-2	0.40	0.18	0.09	0.00	22.8	20.1	21.1	0.0	3.7	2.7	2.4	0.0	0.32
N0936-1	0.34	0.29	0.17	0.09	27.3	36.9	37.5	38.5	8.8	9.4	8.4	7.3	0.19
N0936-2	0.43	0.00	0.00	0.00	42.5	0.0	0.0	0.0	10.0	0.0	0.0	0.0	0.30
N1079.............	0.68	0.28	0.13	0.06	42.4	40.2	39.9	39.9	14.7	8.8	6.3	4.7	0.42
N1302-1	0.30	0.09	0.00	0.00	18.3	20.0	0.0	0.0	5.3	4.7	0.0	0.0	0.16
N1302-2	0.23	0.06	0.00	0.00	30.3	27.4	0.0	0.0	5.3	2.2	0.0	0.0	0.26
N1317.............	0.36	0.18	0.11	0.06	4.7	5.1	5.2	5.3	2.1	1.6	1.3	1.3	0.06
N1326-1	0.08	0.09	0.03	0.04	20.1	26.5	29.9	28.2	4.1	5.6	3.3	5.5	0.18
N1326-2	0.64	0.22	0.09	0.03	41.9	41.5	37.1	39.0	17.3	11.6	10.8	6.4	0.38
N1387.............	0.39	0.15	0.06	0.03	18.3	17.9	17.2	17.0	6.0	5.1	4.9	4.9	0.22
N1440.............	0.48	0.23	0.11	0.05	17.3	18.4	19.4	19.6	6.8	4.7	3.7	4.4	0.26
N1452-1	0.75	0.53	0.43	0.28	20.5	26.8	31.0	31.4	7.3	7.8	8.4	7.7	0.30
N1452-2	0.67	0.36	0.18	0.12	38.3	41.9	43.7	41.6	10.0	7.0	4.3	7.1	0.56
N1533.............	0.42	0.17	0.07	0.03	19.1	20.1	21.7	22.2	7.6	5.9	5.9	6.2	0.24
N1574.............	0.32	0.14	0.06	0.03	13.3	13.5	13.5	13.5	4.3	3.6	3.1	3.7	0.13
N2217.............	0.51	0.25	0.15	0.09	33.4	32.9	34.0	34.5	11.7	9.4	7.4	7.5	0.24
N2273-1	0.20	0.23	0.15	0.08	15.0	18.4	19.1	19.5	3.2	4.8	3.9	3.7	0.14
N2273-2	0.60	0.20	0.06	0.05	30.9	36.0	39.3	41.5	12.1	6.7	6.7	8.2	0.30
N2681.............	0.25	0.06	0.03	0.00	14.9	14.9	14.6	0.0	5.0	3.8	3.2	0.0	0.13
N2781-1	0.47	0.00	0.00	0.00	36.4	0.0	0.0	0.0	8.1	0.0	0.0	0.0	0.43
N2781-2	0.33	0.00	0.00	0.00	54.8	0.0	0.0	0.0	8.4	0.0	0.0	0.0	0.65
N2787.............	0.52	0.21	0.11	0.06	34.3	36.3	36.6	37.3	10.2	7.9	7.2	6.2	0.38
N2859-1	0.56	0.22	0.11	0.06	40.2	39.6	40.2	40.6	13.5	11.7	9.1	8.7	0.32
N2859-2	0.37	0.00	0.00	0.00	66.1	0.0	0.0	0.0	11.6	0.0	0.0	0.0	0.53
N2983-1	0.32	0.44	0.27	0.17	14.9	25.4	25.9	26.4	4.7	7.3	5.9	5.4	0.21
N2983-2	0.74	0.00	0.00	0.00	25.4	0.0	0.0	0.0	7.6	0.0	0.0	0.0	0.35
N3081.............	0.28	0.10	0.05	0.00	5.4	5.3	5.2	0.0	2.0	1.6	1.4	0.0	0.08
N3941.............	0.33	0.14	0.05	0.00	20.4	20.8	20.3	0.0	5.0	3.4	2.6	0.0	0.21
N4245-1	0.28	0.11	0.08	0.05	19.7	23.0	26.3	29.6	6.8	5.3	5.6	4.4	0.23
N4245-2	0.49	0.17	0.09	0.04	38.4	38.1	38.5	38.2	8.7	8.4	4.2	2.5	0.44
N4596-1	0.66	0.26	0.11	0.09	38.6	39.8	39.2	44.5	14.1	8.8	6.9	8.4	0.34
N4596-2	0.45	0.30	0.22	0.12	61.0	57.4	53.8	56.6	8.1	10.4	8.6	6.9	0.54
N4608-1	0.62	0.40	0.32	0.22	25.9	33.1	36.4	37.7	10.8	10.1	9.5	9.3	0.28
N4608-2	0.42	0.12	0.00	0.00	43.3	41.7	0.0	0.0	10.1	9.5	0.0	0.0	0.47
N4643-1	0.85	0.56	0.38	0.25	33.3	39.3	41.0	41.8	13.2	12.1	10.8	10.0	0.36
N4643-2	0.38	0.14	0.10	0.09	54.6	54.7	54.2	53.8	7.9	3.5	3.2	3.8	0.59

NOTES.—Col. (1): Galaxy name. If a double Gaussian was fitted to the I_m/I_0 profiles, the first Gaussian is listed as "-1," while the second is "-2." Cols. (2–5): Gaussian relative amplitudes A_m (eq. [1]) for $m = 2, 4, 6,$ and 8. For a double-Gaussian fit (eq. [2]), A_{1m} is listed on the first line and A_{2m} is listed on the second line for a given galaxy. Cols. (6–9): Mean radii r_m (or r_{1m} and r_{2m} for a double-Gaussian fit) in arcseconds. Cols. (10–13): Gaussian width σ_m (or σ_{1m} and σ_{2m} for a double-Gaussian fit) in arcseconds. Col. (14): Ratio of radius r_2 to the radius $r_o = D_o/2$ of the standard isophote having $\mu_B = 25.00$ mag arcsec^{-2} (from RC3).

For these galaxies, the bar plus background disk/bulge light can be described mathematically as

$$I(r, \phi) = I_0(r)\left[1 + \sum_{m=2}^{4,6,\text{etc.}} A_m e^{-(r-r_m)^2/2\sigma_m^2} \cos m(\phi - \phi_m)\right],$$

(1)

where A_m is a constant, r_m is the mean radius, σ_m is the Gaussian width, and ϕ_m is the phase for each Fourier component m. The parameters of these single-Gaussian representations are summarized in Table 3; for NGC 1317 and 3081, the fits refer to a strong secondary bar.

5.2.2. Double-Gaussian Fourier Profiles

Other galaxies in our sample have lower order I_m/I_0 profiles that are better represented by a double-Gaussian fit. The bars seen in NGC 936, 1452, 2983, 4245, 4596, 4608, and 4643 show this characteristic. For NGC 936 and 2983, only the $m = 2$ term required a double-Gaussian fit, while for NGC 1452 and 4643 even the higher-order terms required double-Gaussian fits. For these galaxies, the bar plus background disk light can be described mathematically as

$$I(r, \phi) = I_0(r)\left[1 + \sum_{n=1}^{2} \sum_{m=2}^{4,6,\text{etc.}} A_{nm} e^{-(r-r_{nm})^2/2\sigma_{nm}^2} \cos m(\phi - \phi_m)\right].$$

(2)

In principle, ϕ_m could be different for the two Gaussian components, but in such a case the two features would not be part of the same bar and would have to be analyzed separately. The parameters of the double-Gaussian representations are also summarized in Table 3, divided into components 1 and 2.

TABLE 4
SUMMARY OF PRIMARY COMPONENTS

Galaxy (1)	Fourier Profile Type (2)	Primary Feature (3)	Other Features (4)	Main Bar Profile Type (5)
NGC 718....................	MCFP	Pointy oval	Detached ansae, extended aligned oval	Intermediate
NGC 936....................	DGFP	Ansae bar		Flat
NGC 1022...................	MCFP	Distorted bar	Oval disk	Intermediate
NGC 1079[a]................	MCFP	Ansae bar	Extended misaligned oval	Flat
NGC 1302...................	DGFP	Pointy oval		Exponential
NGC 1317...................	MCFP	Oval		Intermediate (sec. bar)
NGC 1326...................	MCFP	Ansae bar	Extended aligned oval	Flat
NGC 1387...................	SGFP	Regular bar		Exponential
NGC 1440...................	SGFP	Regular bar		Intermediate
NGC 1452...................	DGFP	Regular bar		Flat
NGC 1512...................	MCFP	Ansae bar	Extended aligned oval	Flat
NGC 1533...................	SGFP	Regular bar	Extended misaligned outer oval	Intermediate
NGC 1574...................	SGFP	Regular bar	Extended misaligned outer oval	Intermediate
NGC 2217...................	SGFP	Regular bar		Flat
NGC 2273...................	MCFP	Ansae bar	Extended aligned oval	Flat
NGC 2681...................	MCFP	Regular bar	Extended misaligned ansae oval	Intermediate
NGC 2781...................	DGFP	Oval	Extended aligned oval	Intermediate
NGC 2787...................	SGFP	Ansae bar		Flat
NGC 2859...................	DGFP	Ansae bar	Inner oval, extended aligned outer oval	Flat
NGC 2983...................	DGFP	Ansae bar		Flat
NGC 3081...................	MCFP	Ring/oval	Aligned intermediate bar	Flat
NGC 3941...................	SGFP	Ansae bar		Intermediate
NGC 4245...................	DGFP	Regular bar	Extended aligned oval	Intermediate
NGC 4596...................	DGFP	Ansae bar	Extended aligned oval	Intermediate
NGC 4608...................	DGFP	Regular bar		Intermediate
NGC 4643...................	DGFP	Regular bar		Intermediate

NOTES.— Col. (1): Galaxy name. Col. (2): Fourier I_m/I_0 profile type based on Gaussian fitting, where SGFP = single Gaussian Fourier profile, DGFP = double Gaussian Fourier profile, and MCFP = multicomponent Fourier profile (§ 5.2). Col. (3): Morphology of primary bar or barlike feature. Col. (4): Additional nonnuclear barlike features. Col. (5): Elmegreen & Elmegreen (1985) primary bar classification.

[a] Deprojection uncertainties complicated analysis; inner regions affected by bulge deprojection stretch.

5.3. Multicomponent Fourier Profiles

The remaining galaxies in our sample show more complicated Fourier profiles compared to the single- and double-Gaussian cases. The presence of rings, multiple bars, extended ovals, and sometimes faint spirals is often the reason why the more simple representations outlined above do not work. Nevertheless, the profiles in these cases can usually be partly interpreted in terms of single or double Gaussians, as shown in Figure 3.

For example, in NGC 718 the bar is an unusual multicomponent type including an inner pointy oval, two bright ansae beyond the ends of this bar, and an extended oval, all in approximately the same position angle. The double-Gaussian fit shown in Figure 4 does not include the extended oval. Beyond a radius of $35''$, faint spiral structure also adds amplitude.

In NGC 1022, the bar shows considerable isophote twisting. We can identify at least two components in this bar in different position angles, and we show an approximate separation in Figure 4 based only on the symmetry assumption and not on Gaussian fits. There is also an outer ring and weak spiral structure outside the bar region.

The primary feature in NGC 1302 is a pointy oval that can be characterized in terms of a double Gaussian with the two components in slightly different position angles. There is extra $m = 2$ and 4 amplitude outside this bar that is very faint and difficult to interpret.

NGC 1317 is an interesting case in which the primary feature is an oval, while the secondary bar is a normal bar in a position angle offset by $90°$. The primary oval shows a relatively sym-

metric multicomponent $m = 2$ profile, while the secondary bar is approximately a single-Gaussian type that does not appear to overlap the primary oval. The two components show Fourier profiles that are completely separated.

All of the amplitude from $10''$ to $80''$ has virtually the same phase in NGC 1326. Its nonaxisymmetry is characterized by an ansae-type primary bar embedded within a highly elongated oval. The Fourier profiles can be represented well with a double-Gaussian fit to the $m = 2$, 4, and 6 terms. The asymmetry in each of these terms changes because the outer Fourier component weakens relative to the inner one with increasing m. There is extra $m = 2$ and 4 light that appears to be due to enhancements in the outer ring along the bar axis.

NGC 1512 is an early-type spiral with a strong primary bar and an elongated inner pseudoring around the bar. The presence of the ring means we cannot study the bar profile alone. Figure 4 shows how we would map the bar using the symmetry assumption. The double-humped mapping completely removes the bar from the image. The remaining amplitude is connected with the oval intrinsic shape of the inner pseudoring.

NGC 2273 is an early-type spiral having a well-defined bar, an inner spiral pseudoring, and an extended oval, all in approximately the same position angle. The double-Gaussian representation shown in Figure 4 provides a good approximation to the bar. The excess $m = 2$ amplitude beyond $r = 40''$ is due to the innermost of the galaxy's two outer rings. This ring is intrinsically aligned perpendicular to the bar and oval.

As already noted, the classified bar in NGC 2681 is mostly a single-Gaussian type, but outside this bar is a significantly

TABLE 5

Mean Fourier Parameters

Parameter (1)	SGFP Cases				DGFP Cases			
	Mean (2)	Standard Deviation (3)	Mean Error (4)	n (5)	Mean (6)	Standard Deviation (7)	Mean Error (8)	n (9)
$\langle r_2 \rangle$ (kpc)	1.76	0.74	0.28	7	2.68	1.31	0.41	10
$\langle \sigma_2 \rangle$ (kpc)	0.58	0.26	0.10	7	0.88	0.38	0.12	10
$\langle r_{22} \rangle$ (kpc)	...	...	...	...	4.39	1.96	0.62	10
$\langle \sigma_{22} \rangle$ (kpc)	...	...	...	...	0.84	0.31	0.10	10
$\langle I_4/I_2 \rangle$	0.43	0.04	0.01	7	0.64	0.33	0.11	9
$\langle I_6/I_2 \rangle$	0.20	0.05	0.02	7	0.44	0.22	0.08	8
$\langle I_8/I_2 \rangle$	0.10	0.04	0.01	6	0.28	0.14	0.05	8
$\langle I_{10}/I_2 \rangle$	0.06	0.03	0.01	6	0.19	0.11	0.04	8
$\langle I_{42}/I_{22} \rangle$	...	...	...	...	0.41	0.16	0.07	6
$\langle I_{62}/I_{22} \rangle$	...	...	...	...	0.30	0.14	0.07	4
$\langle I_{82}/I_{22} \rangle$	...	...	...	...	0.19	0.08	0.04	4
$\langle I_{102}/I_{22} \rangle$	...	...	...	...	0.11	0.07	0.04	3
$\langle r_4/r_2 \rangle$	1.02	0.04	0.01	7	1.23	0.21	0.07	9
$\langle r_6/r_2 \rangle$	1.04	0.07	0.03	7	1.33	0.25	0.09	8
$\langle r_8/r_2 \rangle$	1.06	0.08	0.03	6	1.39	0.24	0.08	8
$\langle r_{10}/r_2 \rangle$	1.12	0.14	0.06	6	1.44	0.25	0.09	8
$\langle r_{42}/r_{22} \rangle$	...	...	...	...	0.98	0.06	0.03	6
$\langle r_{62}/r_{22} \rangle$	...	...	...	...	1.00	0.11	0.05	4
$\langle r_{82}/r_{22} \rangle$	...	...	...	...	1.00	0.07	0.03	4
$\langle r_{102}/r_{22} \rangle$	...	...	...	...	1.04	0.11	0.07	3
$\langle \sigma_4/\sigma_2 \rangle$	0.77	0.07	0.03	7	0.96	0.26	0.09	9
$\langle \sigma_6/\sigma_2 \rangle$	0.68	0.11	0.04	7	0.88	0.24	0.09	8
$\langle \sigma_8/\sigma_2 \rangle$	0.74	0.12	0.05	6	0.81	0.20	0.07	8
$\langle \sigma_{10}/\sigma_2 \rangle$	1.05	0.36	0.15	6	1.18	0.28	0.10	8
$\langle \sigma_{42}/\sigma_{22} \rangle$	...	...	...	...	0.79	0.33	0.14	6
$\langle \sigma_{62}/\sigma_{22} \rangle$	...	...	...	...	0.60	0.31	0.16	4
$\langle \sigma_{82}/\sigma_{22} \rangle$	...	...	...	...	0.58	0.25	0.12	4
$\langle \sigma_{102}/\sigma_{22} \rangle$	...	...	...	...	0.92	0.44	0.26	3
$\langle M_B^o \rangle$	−19.53	0.70	0.26	7	−19.72	0.84	0.27	10

Notes.—Col. (1): Fourier parameter (linear diameters use the distance moduli from Table 1). Cols. (2–5:) Parameter means, standard deviations, mean errors, and number of objects for SGFP cases from Table 4. Cols. (6–9): The same for DGFP cases from Table 4.

extended and somewhat pointy oval in a very different position angle. This oval is a major feature of the galaxy's nonaxisymmetry distribution.

The $m = 2$ profile of NGC 2781 shows an approximately Gaussian peak at $r = 6\rlap{.}''5$ due to a small inner disk in the center, noted by Paper I. Completely separate from this feature is a broad, extended oval with a slightly asymmetric profile. This feature can be well represented by two displaced Gaussians in slightly different position angles. The two Gaussians are shown separately in Figure 4.

NGC 2859 is very similar to NGC 2781 in having a very broad $m = 2$ hump at larger radii. The broad hump includes a significant ansae-type bar and an extended oval. Figure 4 shows a double-Gaussian representation of the two features. Significant $m > 2$ amplitude is found mainly for the inner Gaussian component.

NGC 3081 is the most interesting of the multicomponent cases. One can identify three clear barlike features: a secondary bar, a weak primary bar, and an extended oval in the form of a bright elliptical inner ring (Buta & Purcell 1998). The primary and secondary bars have nearly the same maximum value of I_2/I_0, but the extended oval ring is clearly the dominant nonaxisymmetric feature. The secondary bar is well-represented as a single-Gaussian type.

5.4. Summary of Bar Components

Table 4 summarizes the results of § 5.3. It lists the principal feature seen in the Fourier profiles and any barlike features seen at larger radii. The information listed in column (3) of Table 4 shows that ansae-type bars are as frequent as normal ("regular") bars in this sample. Some of the barred properties are highlighted in Paper I and Paper III, as well as in other publications (e.g., Wozniak et al. 1995; Laine et al. 2002; Erwin 2004).

The results show that Fourier analysis does well in separating bar, oval, and lens structures from spiral arms, with oval and lens structures affecting both double-Gaussian and multicomponent profiles. One of the interesting results from Table 4 is the large fraction of the sample galaxies that have a bar that is *not* associated with a strong extended oval. Cases such as NGC 1387, NGC 1440, and NGC 3941 present some of the purest bars (in Fourier space at least) known. Nevertheless, our two-dimensional decompositions give somewhat different views of the structures seen in some of these galaxies. For example, Paper I and Paper III note that including a lens in the decomposition models of NGC 1387, 1440, 1533, 1574, and 3941 improves the fits (but has no effect on bulge-to-total luminosity ratios); all of these show single-Gaussian Fourier profiles. In some of these cases, the lens in question is more of an outer lens (Kormendy 1979) than an inner lens, and the features have little impact on the Fourier terms because they are not very barlike. In the cases of NGC 1533 and 1574, significant $m = 2$ amplitude is seen outside the bar region (Fig. 4). Fourier decomposition and two-dimensional multicomponent decompositions do not always detect the same structural components because the former is designed to characterize nonaxisymmetric components, while the
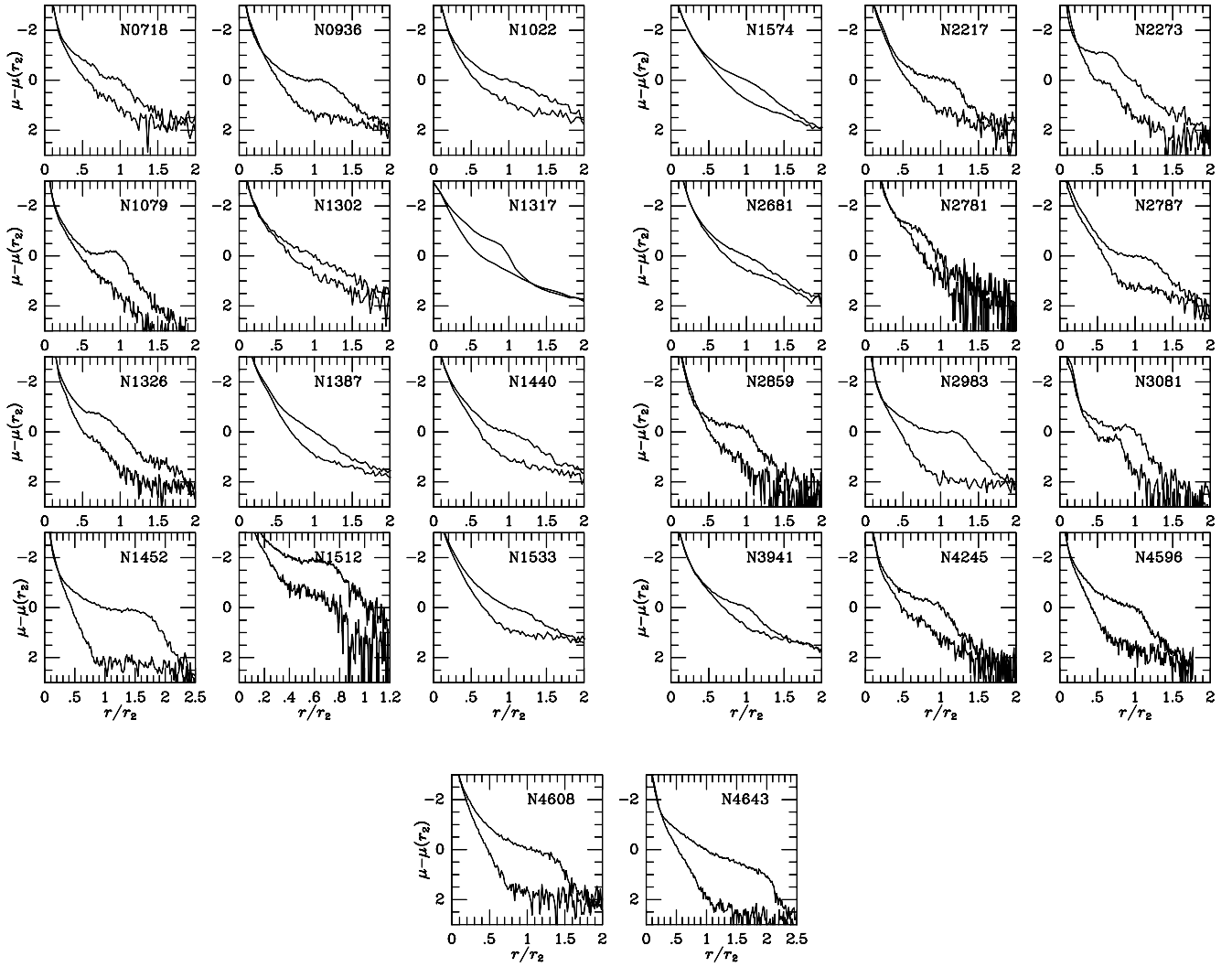
Fig. 7.—Radial surface brightness profiles along the major and minor axes of the main bar. The radii are normalized to the radius r_2 of the $m = 2$ Fourier term, while surface brightness is shown relative to the surface brightness at this same radius. For NGC 1317, the curves shown are for the secondary bar, not the primary oval.

latter must model all components, both axisymmetric and non-axisymmetric. The two approaches are complimentary, and we use Fourier analysis here only to characterize aspects of the bars seen.

In contrast to NGC 1387, 1440, and 3941, many galaxies have bars imbedded in more significant extended ovals. These ovals are often aligned with the main bar, but misalignment is also found. Also, the ovals may lie so far out that they are distinct entities in their own right. NGC 2859 is an example of an ansae-type bar imbedded in a considerably extended, aligned oval, while NGC 1079 is an example of an ansae-type bar in a slightly mis-aligned extended oval. It is important to note that the extended ovals are distinct from their associated bars. As seen in NGC 2859, the main bar has significant higher order Fourier terms, while the extended oval only appears in the $m = 2$ term.

The mean Fourier parameters for the objects fitted with sin-gle or double Gaussians in Table 3 are summarized in Table 5. The results show that bars fitted by single Gaussians on average are shorter than those requiring double Gaussians and have a smaller Gaussian width. The single-Gaussian bars have $\langle r_2 \rangle = 1.8 \pm 0.3$ kpc and $\langle \sigma_2 \rangle = 0.58 \pm 0.10$ kpc, compared to $\langle r_{12} \rangle = 2.8 \pm 0.4$ kpc and $\langle \sigma_2 \rangle = \langle \sigma_{12} \rangle = 0.88 \pm 0.12$ kpc for the double-Gaussian bars. The mean absolute blue magnitudes are nevertheless very similar between the two groups (last line of

Table 5). Single-Gaussian bars have smaller relative Fourier amplitudes of higher order terms and less increase in r_m with in-creasing m as compared to at least the first Gaussian component of the double-Gaussian bars. The Gaussian widths tend to be larger for $m = 2$ than for $m > 2$.

5.5. Elmegreen Bar Classifications

An important additional piece of information is the classifi-cation of these galaxies according to their bar surface brightness profiles. Elmegreen & Elmegreen (1985) showed that bars can be divided into flat and exponential types according to the shapes of these profiles. Figure 7 shows surface brightness profiles along the primary bar major and minor axes for 26 of our sample galax-ies. (The profiles shown for NGC 1317 are for the secondary bar instead.) The profiles are normalized to the radius r_2 (or the max-imum of r_{12} and r_{22}) of the $m = 2$ Fourier term. Also, the surface brightness is shown relative to that at the radius r_2. From these profiles we have derived the classification of the main bar given in column (5) of Table 4. The profiles show a wide range of shapes that includes both of the Elmegreen types, although half of the galaxies are clearly intermediate between flat and exponential. Only two of our sample galaxies are of the exponential type, which is not unexpected given that Elmegreen & Elmegreen (1985) found exponential profiles mainly for later type galaxies. Table 4

TABLE 6
Bar Strengths and Q_b Families

Galaxy (1)	Q_b Family (2)	Q_b (3)	Mean Error (4)
NGC 718..................................	SAB	0.124	0.000
NGC 936..................................	SAB	0.201	0.028
NGC 1022................................	SAB	0.142	0.016
NGC 1079................................	SAB	0.242	0.052
NGC 1302................................	SAB	0.130	0.007
NGC 1317—primary bar	SAB	0.091	0.008
NGC 1317—secondary bar..........	SAB	0.086	0.006
NGC 1326................................	SAB	0.161	0.014
NGC 1387................................	SAB	0.065	0.002
NGC 1440................................	SAB	0.141	0.004
NGC 1452................................	SB	0.416	0.035
NGC 1512................................	SB	0.270	0.015
NGC 1533................................	SAB	0.107	0.002
NGC 1574................................	SAB	0.064	0.006
NGC 2217................................	SAB	0.170	0.008
NGC 2273................................	SAB	0.209	0.001
NGC 2681—inner bar..................	SA	0.039	0.003
NGC 2681—outer oval	SAB	0.061	0.004
NGC 2781................................	SAB	0.066	0.001
NGC 2787................................	SAB	0.182	0.051
NGC 2859................................	SAB	0.105	0.004
NGC 2983................................	SB	0.297	0.007
NGC 3081—primary bar	SAB	0.069	0.001
NGC 3081—primary oval............	SAB	0.153	0.013
NGC 3081–secondary bar...........	SAB	0.066	0.004
NGC 3941................................	SAB	0.085	0.005
NGC 4245................................	SAB	0.180	0.002
NGC 4596................................	SB	0.271	0.061
NGC 4608................................	SB	0.252	0.005
NGC 4643................................	SB	0.299	0.002

Notes.—Col. (1): Galaxy name. Col. (2): Quantitative family estimate following Buta et al. (2005). Col. (3): Maximum relative bar torque based on Gaussian and other mappings. Col. (4): Mean error excluding systematic effects.

also shows that there is no correlation between Elmegreen bar type and the Fourier profile characteristics. However, the ansae-type bars are more often of the flat type than are the regular bars.

5.6. Bar Strengths

Bar strengths provide an additional way of comparing the various Fourier profile categories among our sample galaxies. We have used the gravitational torque approach (Sanders & Tubbs 1980; Combes & Sanders 1981; Buta & Block 2001) to derive the bar strength, Q_b, from our Gaussian-fitted or symmetry-mapped bar images. This parameter is derived assuming a constant mass-to-light ratio and negligible dark matter but allows for the less flattened shape of the bulge and an exponential vertical density distribution having vertical scale height derived from a fraction of the radial scale length. The procedure is described by Laurikainen & Salo (2002) and Laurikainen et al. (2004). From the force in the plane, we derive Q_b as the maximum of the function

$$Q_T(r) = \frac{|F_T(r, \phi)|_{\max}}{\langle |F_R(r, \phi)| \rangle},$$

where $|F_T(r, \phi)|_{\max}$ is the maximum tangential force and $\langle |F_R(r, \phi)| \rangle$ is the azimuthally averaged radial force. The resulting values of Q_b are compiled in Table 6 and differ only slightly from the *total* nonaxisymmetric strength Q_g presented for these galaxies by Paper I and Paper III.

A comparison between Tables 4 and 6 shows that single-Gaussian bars have a lower average Q_b than do double-Gaussian bars. For the seven single-Gaussian cases, $\langle Q_b \rangle = 0.116 \pm 0.049$ (standard deviation), while for 10 double-Gaussian cases, $\langle Q_b \rangle = 0.222 \pm 0.106$ (standard deviation). For the nine remaining cases, $\langle Q_b \rangle = 0.161 \pm 0.068$ (standard deviation) using the main bar feature when multiple components are listed. The results indicate that single-Gaussian bars are weaker on average than double-Gaussian bars, although the two groups overlap somewhat in Q_b.

The "Q_b family" in Table 6 is a quantitative family estimate based on Q_b (Buta et al. 2005). The Q_b family is SA if $Q_b < 0.05$, SAB if $Q_b = 0.05-0.10$, SAB if $Q_b = 0.10-0.20$, SAB if $Q_b = 0.20-0.25$, and SB if $Q_b \geq 0.25$. These ranges were chosen by Buta et al. (2005) to approximate the way these classifications are often made, especially for the underlined types. Interestingly, from Table 2 17 of our galaxies are visually judged to be type SB, while only six are SB from the Q_b family. The bars in these early-type galaxies are not as strong as they look owing to the significant background bulge and disk components in most cases. The strongest bar in our sample is that seen in NGC 1452, with $Q_b = 0.42$. Although this kind of bar strength is not unusual for a late-type spiral, it is exceptional in our early-type galaxy sample.

5.7. Evaluation of the Symmetry Assumption

The symmetry assumption of relative Fourier intensity profiles was used by Buta et al. (2003) as a straightforward way of separating bars from spirals that allows the determination of quantitative bar strength with the effects of spiral arm torques largely removed. The assumption was based on the appearance
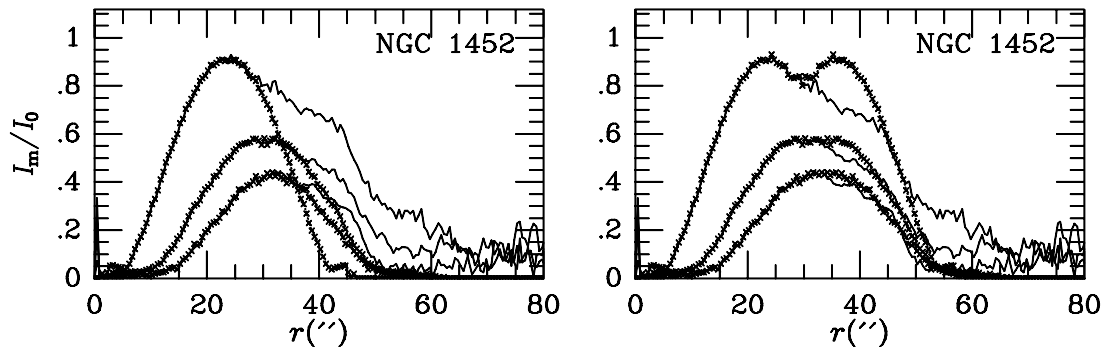

Fig. 8.— Two representations of the bar in NGC 1452 based on application of the symmetry assumption, as opposed to the Gaussian fits shown in Fig. 4. The left panel shows the mapping (crosses) for $r_2 = 24''$, while the right panel shows the mapping for $r_2 = 30''$. The latter resembles what we have used for NGC 1512 in Fig. 4.
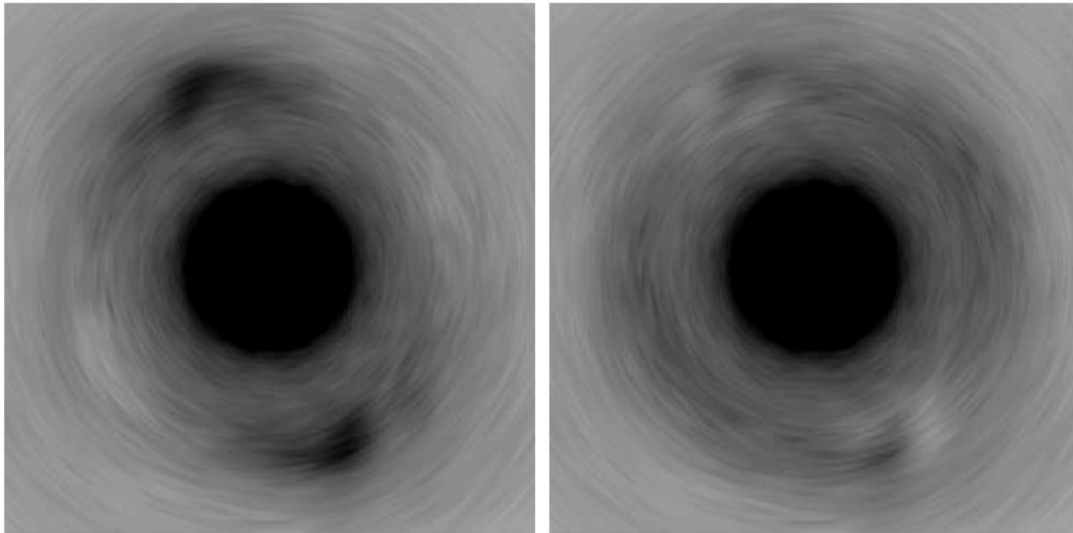
Fig. 9.—Residual intensities in NGC 1452 after removal of the bar mappings in Fig. 8. The left panel is based on $r_2 = 24''$, while the right panel is for $r_2 = 30''$.

of such profiles in the B band for six early-type barred galaxies (NGC 1398, 2217, 4440, 4643, 4650, and 4665; types S0$^+$ to Sab) shown by Ohta et al. (1990). Although first suggested by B-band imaging, the near-IR is still a better band for evaluating this issue because of its reduced sensitivity to dust and star formation.

We have shown that relative Fourier intensity profiles of bars in early-type galaxies show considerable symmetry in some cases and asymmetry in others. Here we evaluate the impact on Q_b of applying the symmetry assumption to two early-type bars with asymmetric I_m/I_0 profiles.

In our sample, NGC 1452 shows a strong case of asymmetry in its bar profile. Figure 8 shows two different applications of the symmetry assumption to the low-order Fourier terms. In the first, the $m = 2$ amplitudes are reflected around $r_2 = 24''$, while in the second these amplitudes are reflected around $r_2 = 30''$. The higher order terms simply follow these mappings, with r_m increasing with m. Figure 9 shows the light remaining after these bar extrapolations are applied. For the $r_2 = 24''$ case (*left panel*), the bar is clearly not fully removed, showing residual ansae. The $r_2 = 30''$ case does a much better removal of the bar. Still, one can see in the map (at the bar ends) where too much bar light has

been removed, as expected. The $r_2 = 30''$ mapping is very similar to what we have used here for NGC 1512. The double-humped representation in that case removes the observed bar from the K_s-band image very well and reveals the spiral arms near the ends of the bar.

To evaluate the impact of the two representations of NGC 1452's bar on bar strength, we have computed Q_b for the double-Gaussian representation in Figure 4 and the two representations in Figure 8. In all three cases, we assumed a vertical scale height of $10''.0$ (1.1 kpc using the distance from Tully 1988). The double-Gaussian fit gives $Q_b = 0.416$ (Table 6), while the $r_2 = 24''$ case gives $Q_b = 0.356$ (14% difference) and the $r_2 = 30''$ case gives $Q_b = 0.432$ (4% difference). Thus, even for an extreme case like NGC 1452, the uncertainty in Q_b introduced by the symmetry assumption is relatively small. In most bar-spiral separations, residuals like those seen in Figure 9 do not occur (Buta et al. 2005).

Next, we apply the symmetry assumption to NGC 4245, a case in which the main peak in the bar might be lost if a strong spiral surrounded the bar. Figure 10 shows the rising portions of the $m = 2$, 4, and 6 profiles reflected around $r = 33''$. This mapping removes most of the bar but leaves two weak enhancements near the bar ends (not shown). The double-Gaussian mapping in Figure 4 gives $Q_b = 0.180$ (Table 6), while the Figure 10 mapping gives $Q_b = 0.174$, a 3% difference.

These two cases demonstrate the effectiveness of the symmetry assumption as a way to separate spiral torques from bars and derive true bar strengths, not only for the majority of galaxies with well-defined, symmetric Fourier profiles but even for those for which the Fourier profiles are less well-behaved, such as NGC 1452 and 4245.

6. DISCUSSION

Interpretation of the results in this paper requires a theory that accounts not only for bar strength and pattern speed but also the varied shapes of bars. Studies by Athanassoula (2005 and references therein) show that angular momentum exchange is at the heart of all of these issues. Critical to the properties of bars is how much angular momentum is transferred to the halo. The effect depends on the density of matter in halo resonances and on how cold or hot the resonant material is. In order to absorb angular momentum a halo must be "live," as opposed to a rigid halo that cannot interact with other galaxy components. Cold, live halos can
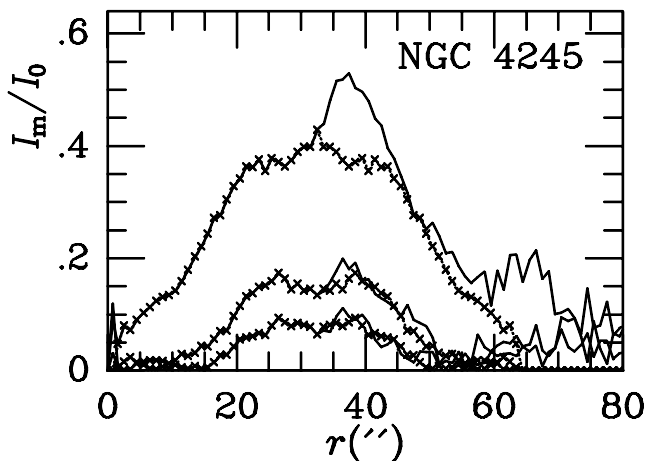

Fig. 10.—Representation of the bar in NGC 4245 based on application of the symmetry assumption (*crosses*), as opposed to the Gaussian fits shown in Fig. 4.

absorb so much angular momentum that a bar can grow very strong. Weaker bars form in warmer, smaller halos or rigid halos, while in hot disks mainly ovals will form. The extreme effects of a live halo interaction have led to the possibility that bars might be found in systems lacking a background disk in the bar region. Gadotti & de Souza (2003) present two possible cases of this, although Paper I presents contrary evidence that does not support their claim.

Athanassoula (2003) computes relative Fourier mass profiles for her models that can be compared to the I_m/I_0 profiles presented in this paper. Provided that the mass-to-light ratio in the K_s band is relatively constant, such a comparison should be fair. The problems of comparing n-body models with real bars are summarized by Athanassoula & Misiriotis (2002), who discuss the types of bars that develop in massive halo (MH), massive disk (MD), and intermediate models. Considering that the models are not of any specific galaxy and are only a few of a large number of models actually computed, the relative Fourier mass profiles well resemble the observed profiles for some of our galaxies. The MH models show strong $m = 2, 4, 6,$ and 8 components, while these are much weaker for the MD models, with $m = 6$ and 8 being in the noise. The MH profiles most resemble those for NGC 1452, 2983, 4608, and 4643 in our sample. The model bars have a fairly sharp outer edge, as is seen in these galaxies.

Athanassoula (2003) shows how the mass of the halo impacts the Fourier terms. More massive halos lead to stronger bars. Her most massive halo model ($M\gamma3$) has Fourier profiles similar to those of NGC 1452 and 4643, two of the strongest bars in our sample. Model MH1, with a less massive halo, has profiles similar to NGC 936 and 2787, while model MH2, with the lowest halo mass in the three illustrated, shows mainly an oval bar and has profiles resembling those of NGC 1302 and 2781.

The good agreement between the models and the observations is further shown by the simulations of Athanassoula et al. (2005), who evaluate the effects of a central mass concentration (CMC) on the evolution of the bar models in the previous papers. They show that a CMC has an effect on the higher m terms, weakening their importance and leading to more $m = 2$–dominated bars. Before the introduction of a CMC in their MH models, the relative Fourier mass profiles (their Fig. 4) strongly resemble those we observe for NGC 4643, which has the sharpest outer edge of all the bars in our sample. In this model, the mass ratios $A_4/A_2 = 0.69$, $A_6/A_2 = 0.47$, and $A_8/A_2 = 0.36$ are very comparable with the intensity ratios found using the first Gaussian component of NGC 4643: $I_4/I_2 = 0.66$, $I_6/I_2 = 0.45$, and $I_8/I_2 = 0.29$, respectively (from Table 3). Comparable values are found for NGC 1452 and NGC 4608. In their MH models with a CMC, the profiles are more symmetric and the ratios above are considerably reduced. This is as observed for most of the other galaxies in our sample whose bars are weaker. MD models in this paper also show similar effects, but the bars are weaker than for the MH models, and the profile asymmetries are less important.

Bureau & Athanassoula (2005) present three n-body models designed for deducing diagnostics of edge-on bars. These models are similar to those used by Athanassoula & Misiriotis (2002) and include a weak bar, an intermediate-strength bar, and a strong bar, with each model bar surrounded by a strong (and largely circular) stellar inner ring. The Fourier decompositions of these barred galaxy models again resemble the galaxies described above. In the strong-bar model, the outer end of the bar has a sharp edge, similar to what is seen in NGC 1452 and 4643 in our sample. The strongest circular inner rings in our sample are seen in NGC 1452 and

4608 (Fig. 2). Weaker circular inner rings are seen in NGC 936, 1317, and 2787, but in several of our galaxies the rings are highly elongated. Early-type barred galaxies have a wide range in intrinsic inner ring shapes, as is typical of such features (Buta 1995).

The relative Fourier intensity profiles of the bars in our sample could also include some of the effects of bar destruction. The bars in our sample that include overlapping extended ovals could be cases in which the bar destruction was in progress at the time the galaxies became relatively deficient in gas. Bournaud & Combes (2002) suggested that bar destruction in the absence of external gas accretion can lead to an oval lens feature (see also Kormendy 1979). An extreme example of this in our sample could be NGC 2859, where the impact of the oval lens extends considerably beyond the ends of the bar. Our Fourier analysis is efficient for separating the lens from the bar in this case, based on the disappearance of the higher order Fourier modes in the lens. Such an extended oval is only weakly seen in NGC 1452, 4608, or 4643, as if these bars were at their peaks and had not begun to disintegrate. These same three galaxies also have little or no central oval or secondary bar.

7. CONCLUSIONS

We have described a new survey designed to study the near-IR properties of bars in early-type (S0−Sa) disk galaxies. The goal of the survey is to obtain a statistically useful database that is comparable in size to that of the Ohio State University survey of bright spiral galaxies, for the principal purpose of deriving the distribution of bar strengths in S0−Sa galaxies. Paper I has presented a multicomponent decomposition analysis of 24 galaxies in our sample obtained thus far. Adding in a number of galaxies observed with the ESO NTT (Paper III), we have examined in this paper the relative Fourier intensity profiles of the bars in a subset of 26 early-type galaxies for which the multicomponent decomposition analysis provided deprojected images.

The results show that a significant fraction (17 out of 26) of the bars in our sample have simple relative Fourier intensity profiles that can be described in terms of single or double Gaussians. The single-Gaussian Fourier profile types represent the simplest types of bars. The presence of extended ovals, secondary bars, and nuclear ovals, as well as intermediate types of features, complicates many of the observed profiles. There is an indication in our sample that single-Gaussian bars are weaker on average than double-Gaussian bars.

Although Gaussians can represent the I_m/I_0 profiles of some bars, the exact physical significance of such representations is unclear at the moment. Nevertheless, numerical bar models reproduce the types of Fourier profiles we observe in our early-type galaxy sample. We have shown that the profiles of the strongest bars in our sample resemble those found for massive halo models of barred galaxies in which the angular momentum exchange between a bar and a massive live halo can be very effective. The weaker bars in our sample may show the effects of CMCs, have hotter and smaller halos, or just have more massive disks than the stronger bars. In any case, it is clear that I_m/I_0 profiles provide a fruitful way of comparing models and simulations and that further such comparisons may clarify the relative importance of different effects.

We have shown that early-type galaxy bars support the symmetry assumption used in bar-spiral separation studies. Even in an extreme case of very asymmetric I_m/I_0 profiles, the use of the symmetry assumption will likely lead to less than a 10% uncertainty in the estimates of relative bar torque strength Q_b (BBK03).

REFERENCES

Aaronson, M., Huchra, J., Mould, J., Schechter, P. L., & Tully, R. B. 1982, ApJ, 258, 64
Athanassoula, E. 2003, MNRAS, 341, 1179
———. 2005, Celest. Mech. Dyn. Astron., 91, 9
Athanassoula, E., Lambert, J. C., & Dehnen, W. 2005, MNRAS, 363, 496
Athanassoula, E., & Misiriotis, A. 2002, MNRAS, 330, 35
Block, D. L., Bournaud, F., Combes, F., Puerari, I., & Buta, R. 2002, A&A, 394, L35
Bournaud, F., & Combes, F. 2002, A&A, 392, 83
Bureau, M., & Athanassoula, E. 2005, ApJ, 626, 159
———. 1995, ApJS, 96, 39
Buta, R., & Block, D. L. 2001, ApJ, 550, 243
Buta, R., Block, D. L., & Knapen, J. H. 2003, AJ, 126, 1148 (BBK03)
Buta, R., Corwin, H. G., & Odewahn, S. C. 2006, The de Vaucouleurs Atlas of Galaxies (Cambridge: Cambridge Univ. Press), in press
Buta, R., Laurikainen, E., & Salo, H. 2004, AJ, 127, 279 (BLS04)
Buta, R., & Purcell, G. B. 1998, AJ, 115, 484
Buta, R., Vasylyev, S., Salo, H., & Laurikainen, E. 2005, AJ, 130, 506
Combes, F., & Sanders, R. H. 1981, A&A, 96, 164
de Vaucouleurs, G. 1959, Handb. Phys., 53, 275
———. 1963, ApJS, 8, 31
de Vaucouleurs, G., et al. 1991, Third Reference Catalog of Bright Galaxies (New York: Springer)
Elmegreen, B. G., & Elmegreen, D. M. 1985, ApJ, 288, 438
Erwin, P. 2004, A&A, 415, 941
Eskridge, P., et al. 2002, ApJS, 143, 73
Gadotti, D. A., & de Souza, R. E. 2003, ApJ, 583, L75

Hubble, E. 1926, ApJ, 64, 321
———. 1936, The Realm of the Nebulae (New York: Dover)
Kormendy, J. 1979, ApJ, 227, 714
Kormendy, J., & Kennicutt, R. C., Jr. 2004, ARA&A, 42, 603
Kormendy, J., & Norman, C. A. 1979, ApJ, 233, 539
Laine, S., Shlosman, I., Knapen, J. H., & Peletier, R. F. 2002, ApJ, 567, 97
Laurikainen, E., & Salo, H. 2002, MNRAS, 337, 1118
Laurikainen, E., Salo, H., & Buta, R. 2004a, ApJ, 607, 103 (LSB04)
———. 2005, MNRAS, 362, 1319 (Paper I)
Laurikainen, E., Salo, H., Buta, R., Knapen, J. H., Speltincx, T., & Block, D. L. 2006, AJ, in press (Paper III)
Laurikainen, E., Salo, H., Buta, R., & Vasylyev, S. 2004b, MNRAS, 355, 1251
Ohta, K., Hamabe, M., & Wakamatsu, K. 1990, ApJ, 357, 71
Persson, S. E., Murphy, D. C., Krzeminski, W., Roth, M., & Rieke, M. J. 1998, AJ, 116, 2475
Press, W. H., Flannery, B. P., & Teukolsky, S. A. 1986, Numerical Recipes: The Art of Scientific Computing (Cambridge: Cambridge Univ. Press)
Quillen, A. C., Frogel, J. A., & González, R. A. 1994, ApJ, 437, 162
Sandage, A. R. 1961, The Hubble Atlas of Galaxies (Washington: Carnegie Inst.)
Sandage, A., & Bedke, J. S. 1994, The Carnegie Atlas of Galaxies (Washington: Carnegie Inst.) (SB94)
Sanders, R. H., & Tubbs, A. D. 1980, ApJ, 235, 803
Tully, R. B. 1988, Nearby Galaxies Catalogue (Cambridge: Cambridge Univ. Press)
Wozniak, H., Friedli, D., Martinet, L., Martin, P., & Bratschi, P. 1995, A&AS, 111, 115